Simulation of 3D DC Borehole Resistivity Measurements with a Goal-Oriented *hp* Finite-Element Method. Part I: Laterolog and LWD

D. Pardo[1], M. Paszynski[2], C. Torres-Verdín[1], and L. Demkowicz[1]

[1]Department of Petroleum and Geosystems Engineering,
1 University Station, C0300,
The University of Texas at Austin,
78712 Austin, TX, USA.
Email:dzubiaur@gmail.com; cverdin@uts.cc; utexas.edu; leszek@ices.utexas.edu
[2]AGH University of Science and Technology
Al.Mickiewicz 30, 30-059, C2-319,
Krakow, Poland
Email: paszynsk@agh.edu.pl

Abstract

We simulate and study the combined three-dimensional effects on resistivity logging measurements due to dip angle (in deviated wells), different arrangements of three-dimensional electrodes, and anisotropy effects. All results correspond to electrostatic (zero frequency) measurements. Thus, we consider direct current (DC) electrodes. We simulate both laterolog and logging-while-drilling (LWD) measurements.

These simulations are performed by considering optimal *hp*-grids obtained from a 2D self-adaptive goal-oriented *hp*-finite element (FE) method, and transferring these grids to a 3D *hp*-FE software. Then, we perform 3D simulations (employing 2D optimal grids) using the 3D software. Finally, an analysis of the error is performed by considering a finer (globally *p*-refined) grid.

Numerical results illustrate the accuracy of the simulations, and indicate that LWD-type measurements (at zero frequency) are more sensitive to dip angle, different arrangements of electrodes, and anisotropy effects than laterolog-type measurements. While vertical well measurements may be insensitive to different electrode configurations and anisotropy effects, for highly deviated wells, consideration of the exact electrode geometries and anisotropy effects may become crucial for the correct interpretation of the results. Thus, all these 3D effects are considered simultaneously, rather than as a superposition of individual effects.

1. Introduction

During the last two decades, different numerical methods have been utilized to simulate three-dimensional (3D) resistivity logging measurements for the assessment of rock formation properties. Among the most widely used methods, we encounter finite-difference schemes using Krylov-based subspace solvers (see, for example, [1-6]). Other methodologies include the use of integral equations (see, for example, [7]), non-orthogonal coordinate systems [8], and finite elements. These methodologies have been applied to study a number of individual 3D effects

such as the sensitivity with respect to different antenna geometries, or results concerning deviated well measurements.

In contrast to previous studies, in this paper we simulate the *combined effect* of logging measurements in presence of deviated wells with anisotropy formation layers and different arrangements of electrodes. As it will be shown in Section 4, this *combined effect* differs from the superposition of individual effects. To achieve this objective, we employ a new numerical methodology based on the use of a 3D *hp* finite element method (FEM) that allows local variations of element size h and polynomial order of approximation, p. Thus, it supports arbitrarily *hp*-refined meshes.

To allow for high contrasts in resistivities and the use of non-cylindrical geometries, we employ exact geometry elements in conformal grids. This feature makes unnecessary both the use of cylindrical coordinates [6] and resistivity averaging techniques [4].

Another unique feature of our methodology consists of using computer-generated adaptive grids according to the following strategy: First, we consider an axi-symmetric model problem associated with our original 3D problem. Then, a two-dimensional (2D) self-adaptive goal-oriented *hp*-FEM [9-12] is used to construct an optimal 2D *hp*-grid. This grid is transferred into the 3D *hp*-FEM software. The original 3D problem is solved for different logging positions by considering the optimal 2D *hp*-grid. Finally, an analysis of the error is performed by considering a finer (globally p-refined) 3D grid. By utilizing this mesh-generation strategy, we avoid the use of human-made *a priori* grids, as the ones presented in [4] (Lebedev's grids) and [13] (staggered grids).

Because of the reduced size of the optimal *hp*-grids generated by the two-dimensional software, we are able to efficiently (1-5 minutes per logging position) simulate our applications with direct solvers, as opposed to iterative solvers as the ones presented in [1-3]. Nevertheless, our *hp*-FE method may also incorporate iterative solvers for increased performance [14].

The remainder of this paper is organized as follows: In Section 2, we introduce our logging applications of interest, which are solved using the *hp*-FE methodology described in Section 3. Then, in Section 4 we describe the corresponding numerical results, with the conclusions presented thereafter.

The numerical methodology described in this paper can be extended to alternate current (AC) logging devices. The corresponding numerical results shall be presented in a forthcoming paper.

2. Problems of interest

In this section, we describe our two logging applications of interest. First, we introduce the physical equation governing our applications and the corresponding variational formulation. Then, we describe two axi-symmetric problems, that shall be later extended to non-axi-symmetric problems by considering dip angles and 3D electrodes.

The model logging instruments considered in this paper are not actual existing instruments. Nevertheless, they operate based on the same physical principles as existing resistivity logging instruments, since we consider similar mandrel and borehole electrical properties, we measure the second vertical difference of the potential, and we also employ patched electrodes. Thus, results are qualitatively similar to those obtained with actual resistivity logging instruments.

2.1. DC resistivity logging

DC resistivity logging applications are governed by the continuity equation at zero frequency, given by

$$-\nabla \cdot \bar{\bar{\sigma}} \nabla u = \nabla \cdot \mathbf{J}, \tag{1}$$

where **J** denotes a prescribed, impressed current source, $\bar{\bar{\sigma}}$ is the conductivity tensor, and u is the electrostatics scalar potential, that is related to the electric field **E** by the relationship

$$\mathbf{E} = -\nabla u \tag{2}$$

Multiplying eq. (1) by a test function, integrating by parts in our computational domain, and incorporating the essential (Dirichlet) and natural (Neumann) boundary conditions defined on Γ_D and Γ_N, respectively — two pieces of the boundary of our computational domain —, we arrive at the following variational problem in terms of the scalar potential u:

$$\begin{cases} \text{Find } u \in u_D + H_D^1(\Omega) \text{ such that:} \\ \int_\Omega \bar{\bar{\sigma}} \nabla u \nabla \xi dV = \int_\Omega \nabla \cdot \mathbf{J} \xi dV + \int_\Omega g \xi dS \quad \forall \xi \in H_D^1(\Omega), \end{cases} \tag{3}$$

where $H_D^1(\Omega) = \left\{ u \in L^2(\Omega) : u|\Gamma_D = 0, \nabla u \in \left(L^2(\Omega)\right)^3 \right\}$ is the space of admissible test functions associated with problem (3), u_D is a lift (typically $u_D = 0$) of the essential boundary condition data u_D (denoted with the same symbol), $g = \bar{\bar{\sigma}} \frac{\partial u}{\partial n}$ is a prescribed flux on Γ_N, and n is the unit normal outward (with respect) vector.

2.2. Axi-symmetric problems

Using cylindrical coordinates (ρ, φ, z), we consider a laterolog-type and logging-while-drilling (LWD)-type axisymmetric problems, with the geometry, sources, receivers, and materials described in Fig.1. For each problem, we shall consider both the case of an anisotropic formation (as illustrated in Fig. 1) and an isotropic formation. For the isotropic case, we consider the formation layers illustrated in Fig. 1, with the exception that for this case, the layer located at 0 m<z<1 m is formed of an isotropic material with resistivity being equal to 0.1 Ωm.

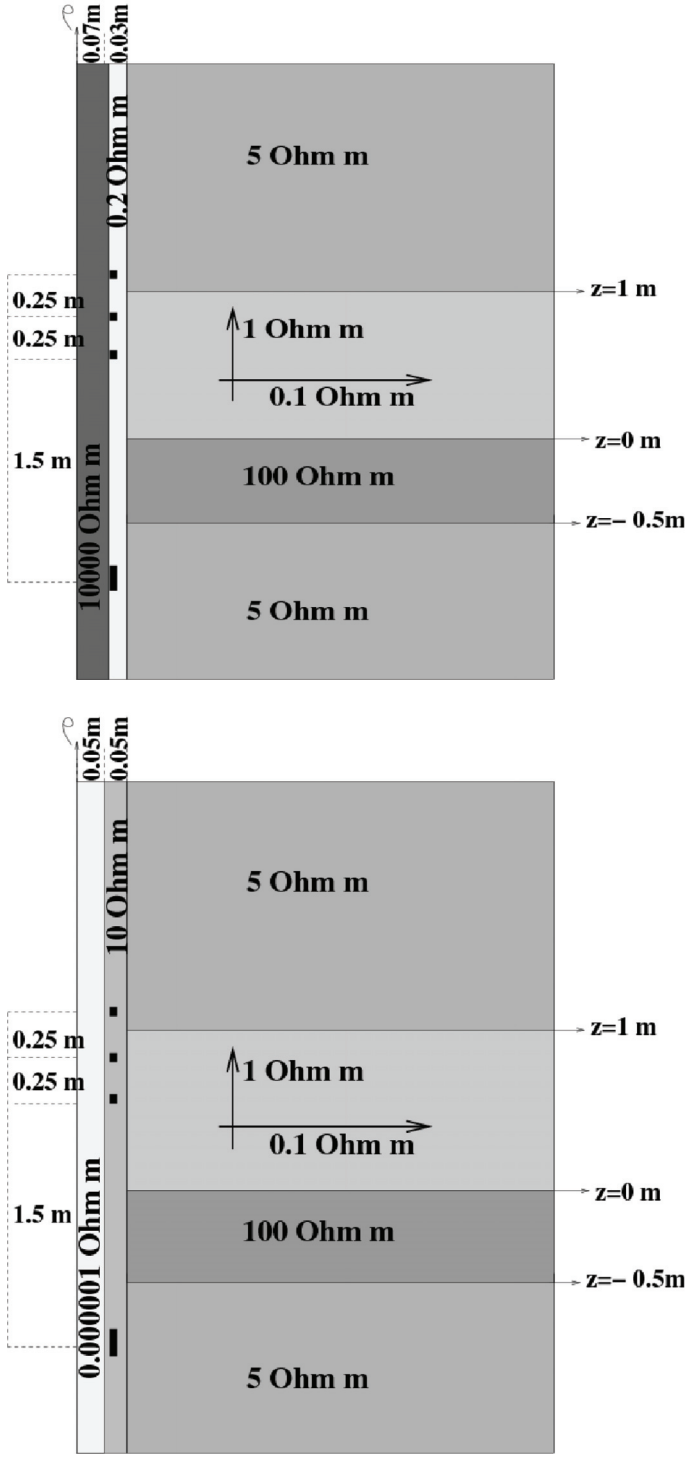

Fig. 1. 2D cross-section of the geometry of the laterolog-type (top panel) and LWD-type (bottom panel). Each problem is composed of a mandrel, a borehole, four different layers in the formation with varying conductivities, one transmitter electrode, and three receiver electrodes.

2.3. 3D problems

At this point, we consider the two axi-symmetric problems described above with a possibly non-zero dip angle, and three different types of electrodes:

1) A ring (axi-symmetric) electrode.
2) An electrode composed of four patches (see Fig. 2 — left panel —).
3) An electrode composed of one-patch (see Fig. 2 — right panel —). The patch for each of the receivers is located on the side opposite to the transmitter patch.

The selected impressed voltage is equivalent for each of the three different types of electrodes considered in this work. Thus, numerical results corresponding to different types of electrodes can be compared among themselves.

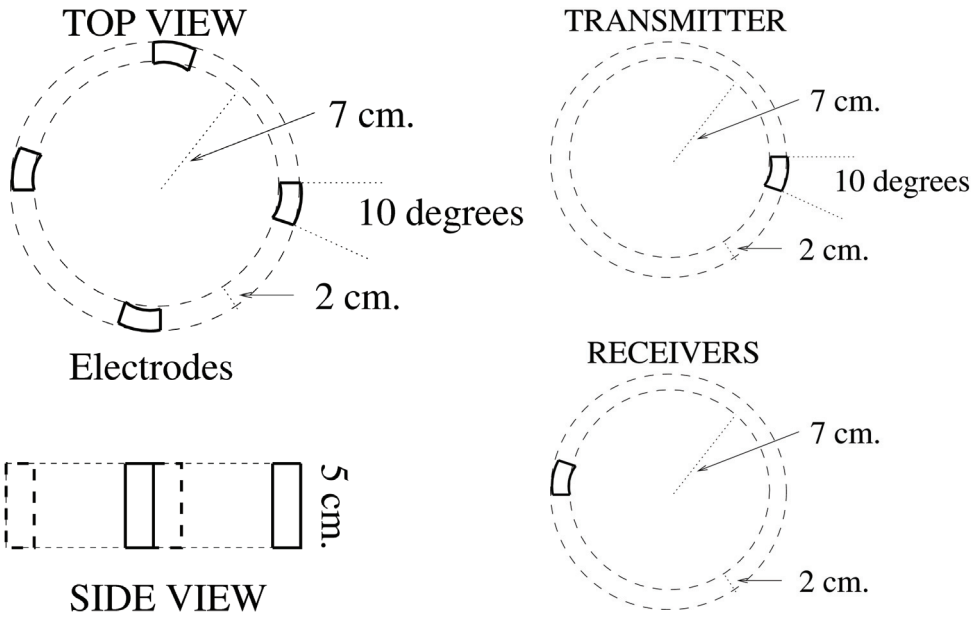

Fig. 2. Geometry of electrodes. Left panel: Top view and side view of the four-patch electrode. Right panel: Top view of the transmitter and receivers one-patch electrodes.

The objective of these simulations is to compute the second vertical difference (without normalization) of the scalar potential at the receiver electrodes.

3. Methodology

Our numerical technique is based on *hp*-FE discretizations of electromagnetic (EM) problems. Here h stands for element size, and p denotes the polynomial element order (degree) of approximation, both varying *locally* throughout the grid.

We combine the use of *hp*-FE discretizations with exact geometry elements and conformal grids. Thus, we avoid geometry-induced numerical errors. Finally, for the problems described above, we construct our *hp*-grids by following the next steps: First, we automatically generate a 2D optimal *hp*-grid for axi-symmetric problems by utilizing the self-adaptive goal-oriented *hp*-FE method described in [9-12]. Notice that the self-adaptive algorithm has the unique feature of

providing exponential convergence rates in terms of the error (in the quantity of interest) vs. the CPU time[2] , independently of the number or intensity of the singularities present in the solution. Second, we transfer the optimal 2D grid to the 3D *hp*-FE software by employing either four or eight second-order elements in the azimuthal direction. Third, the resulting 3D *hp*-FE grid is tilted to account for deviated wells. For different arrangements of electrodes, the load is also modified accordingly. Finally, and after solving our problem of interest within the 3D *hp*-FE software setting, an analysis of the error is performed by considering a finer (globally *p*-refined) 3D grid and by comparing results for both grids.

4. Numerical results

In this section, we present the final simulated borehole measurements corresponding to our Laterolog and LWD problems of interest at DC.

4.1. Laterolog-type measurements

In Fig. 3 — top panel — we display results corresponding to the isotropic case and full-ring electrodes for the axi-symmetric problem — left panel — and the sixty-degree deviated well — right panel —. Results indicate a slight shift and lower readings for the most conductive layer of the formation for the case of a deviated well. This lower intensity reading in the most conductive layer of the deviated well occurs because, physically, the average conductivity σ along the most conductive layer in the plane perpendicular to the well is lower in deviated wells. If we consider the one-patch electrodes described in Section 2, we observe (see Fig. 3 — bottom panel —) almost identical results for the case of a vertical well. For the sixty-degree deviated well, we observe a slight shift on the readings corresponding to the most conductive layer with respect to the results for the vertical well. We note that results for the sixty-degree deviated well increase by about 75% when we consider the one-patch electrodes as opposed to the full-ring electrodes. This remark can be further appreciated in Fig. 4 — top-right panel —. For vertical wells or for electrodes composed of four patches, results are similar to those obtained by considering full-ring electrodes.

In Fig.4 — bottom panel —, we display the simulated logs corresponding to the case when the most conductive layer of the formation is anisotropic, as indicated in Section 2. For vertical wells, these effects are non-existing. However, for a sixty-degree deviated well, anisotropy effects produce 20% larger readings across the most conductive layer of the formation, since the conductivity value in the direction parallel to the well is larger in deviated wells.

To summarize, the effects of anisotropy and different types of electrodes in laterolog-type measurements are only significant in highly-deviated wells. For vertical wells, different arrangements of electrodes do not produce measurable differences.

4.2 LWD-type measurements

Results of Fig. 5 indicate that LWD-type measurements are more sensitive to variations of conductivity of the formation when we consider a vertical well as opposed to a sixty-degree deviated well. This observation holds true for full-ring electrodes as well as for electrodes

2) The self-adaptive *hp*-FE method delivers exponential convergence rates in terms of the error vs. the number of unknowns (see, for example, [12]). The CPU time is a polynomial function of the number of unknowns (linear for multigrid solvers, and quadratic for direct solvers). Since the composition of an exponential function with a polynomial function produces an exponential function, we conclude that the convergence of the error is exponential with respect to the CPU time.

composed of four patches. Again, we observed averaged readings in deviated wells, since physically, measurements correspond to the average conductivity along the plane perpendicular to the well.

For a thirty-degree deviated well, results are similar to those obtained for a vertical well (see Fig. 6 — top left panel —). For the case of electrodes composed of one-patch in a sixty-degree deviated well, we observe a substantial shift in all readings, accompanied by a larger sensitivity — than with any of the other types of electrodes considered in this study — with respect to the conductivity of the formation. Physically, for one-patch electrodes, measurements are proportional to the averaged conductivity σ in the direction perpendicular to the well and along the azimuthal angle where the electrode patch is present.

In Fig 6 — bottom panel — we observe the dramatic effect that anisotropy has on the results for the case of deviated wells. First, the sensitivity with respect to the resistivity of the formation increases by about 100%. At the same time, the effects of anisotropy in the most conductive layer is non-local, and it affects the results across the whole log interval considered in the study.

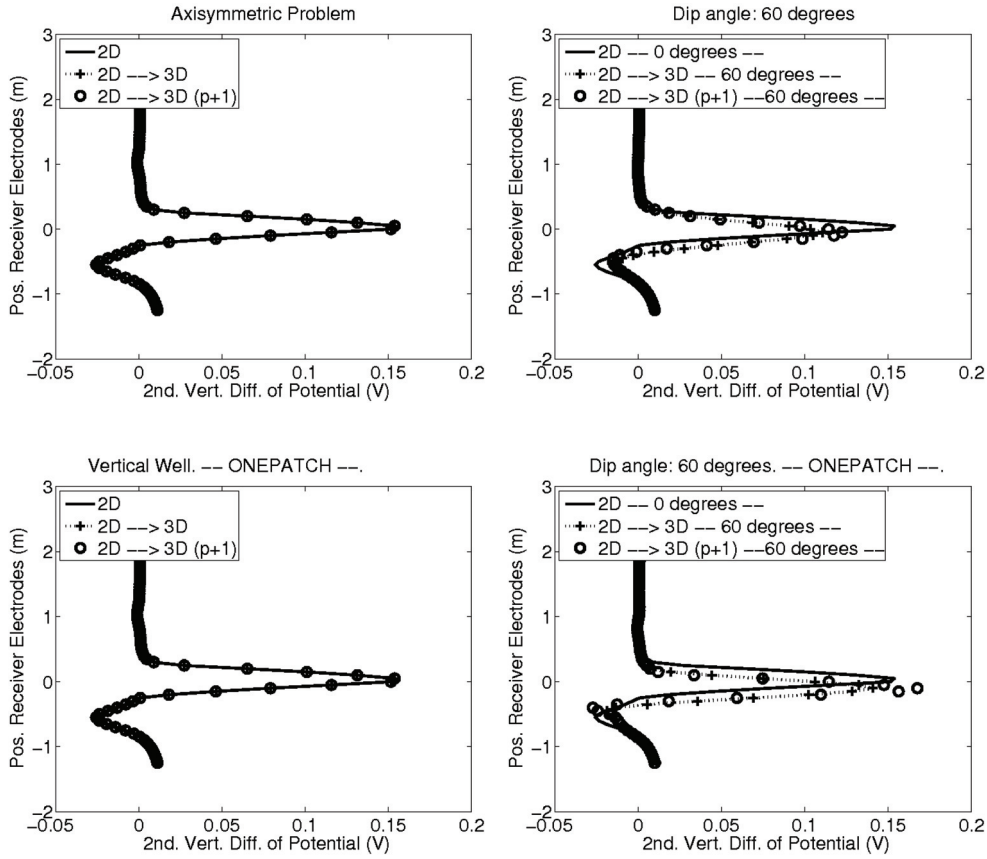

Fig. 3. Laterolog problem, isotropic case. Different curves identify the following results: A) Continuous line: Results obtained with the 2D *hp*-FE software. B) Discontinuous line with '+': Results obtained using an optimal 2D *hp*-FE grid transferred to the 3D software. C) Circles 'o': Results obtained with an optimal 2D *hp*-FE grid transferred to the 3D software, and increase globally the polynomial order of approximation *p* by one. Left panel: Vertical well; Right panel: 60-degree deviated well. Top panel: full ring electrodes; Bottom panel: one-patch electrodes.

To summarize, the effects of anisotropy and different types of electrodes in LWD-type measurements (at zero frequency) are only significant in highly-deviated wells. For vertical wells, different arrangements of electrodes do not produce significant differences in the measurements. This observation for vertical wells agrees with the study performed in [6]. Nevertheless, consideration of anisotropy effects and different electrode configurations in highly-deviated wells becomes crucial for the correct interpretation of the corresponding measurements.

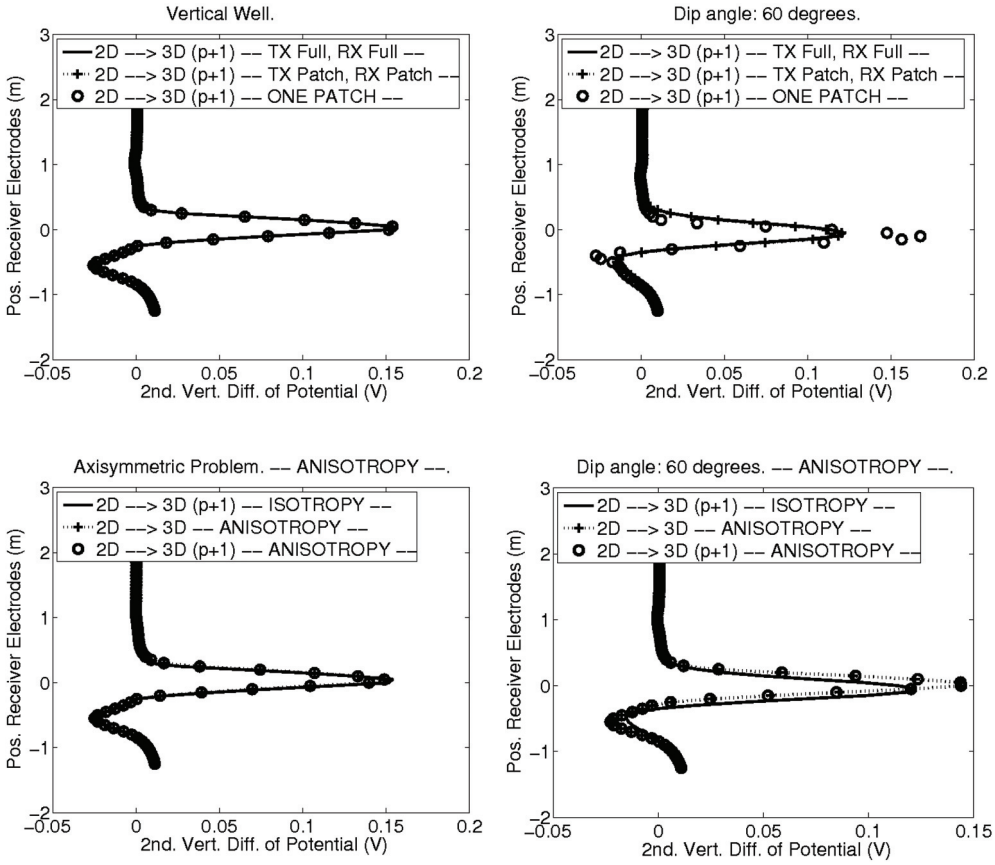

Fig. 4. Laterolog problem. Left panel: Vertical well; Right panel: 60-degree deviated well. Results obtained using an optimal 2D *hp*-FE grid transferred to the 3D software, and possibly increase globally the polynomial order of approximation *p* by one. Top panel: Different curves identify the following electrode configurations: A) Continuous line: Full-ring electrodes. B) Discontinuous line with '+': Electrodes composed of four patches. C) Circles 'o': Electrodes composed of one-patch. Bottom panel: Different curves identify the following results: A) Continuous line: Isotropic problem. B) Discontinuous line with '+': Anisotropic problem. C) Circles 'o': Anisotropic problem, and global increase globally of the polynomial order of approximation *p* by one.

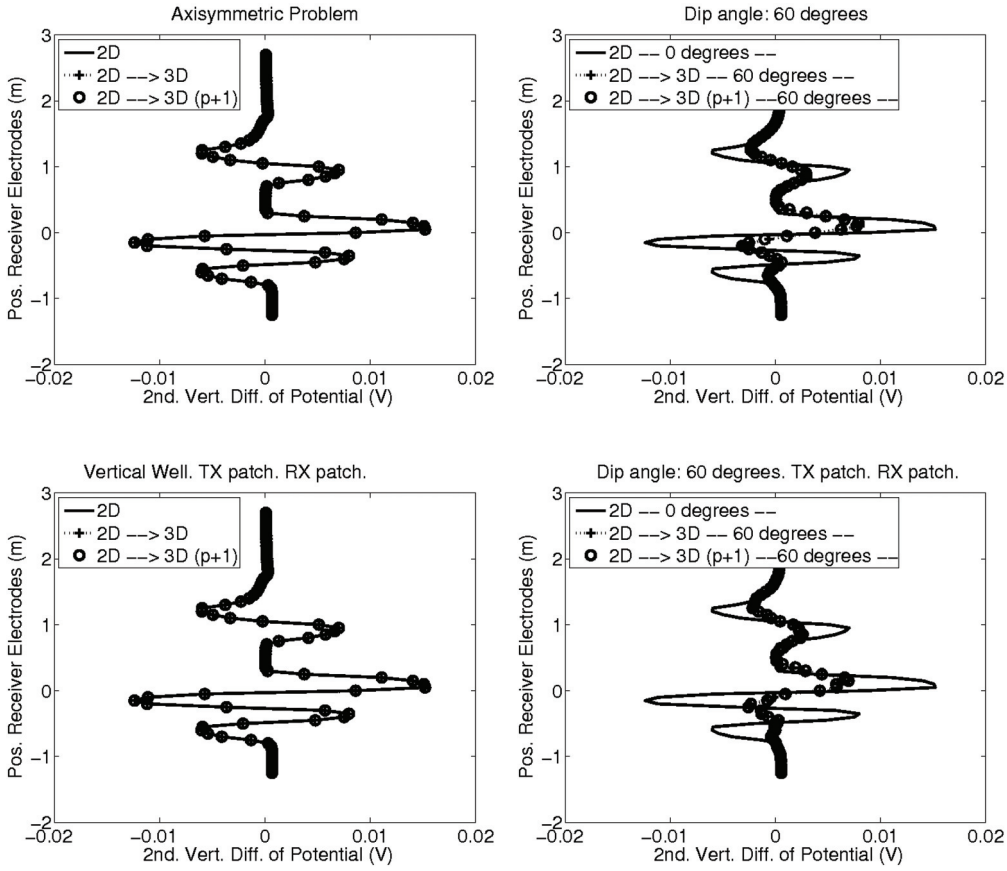

Fig. 5. LWD problem, isotropic case. Different curves identify the following results: A) Continuous line: Results obtained with the 2D *hp*-FE software. B) Discontinuous line with '+': Results obtained using an optimal 2D *hp*-FE grid transferred to the 3D software. C) Circles 'o': Results obtained with an optimal 2D *hp*-FE grid transferred to the 3D software, and increase globally the polynomial order of approximation *p* by one. Left panel: Vertical well; Right panel: 60-degree deviated well. Top panel: full-ring electrodes; Bottom panel: four-patch electrodes.

5. Conclusions

We have analyzed a number of combined 3D effects on borehole DC resistivity measurements. Results clearly indicate that it is essential to consider the combined effects rather than the superposition of individual effects. In particular, for a number of electrode configurations and anisotropic formations whose effects are negligible in vertical wells, we observe that they dramatically modify measurements for the case of highly-deviated wells.

Numerical results also indicate that LWD-type measurements (at zero frequency) are more sensitive to different electrode configurations and anisotropy effects than Laterolog-type measurements. We have also observed that sensitivity with respect to formation conductivity decreases as we increase the dip angle.

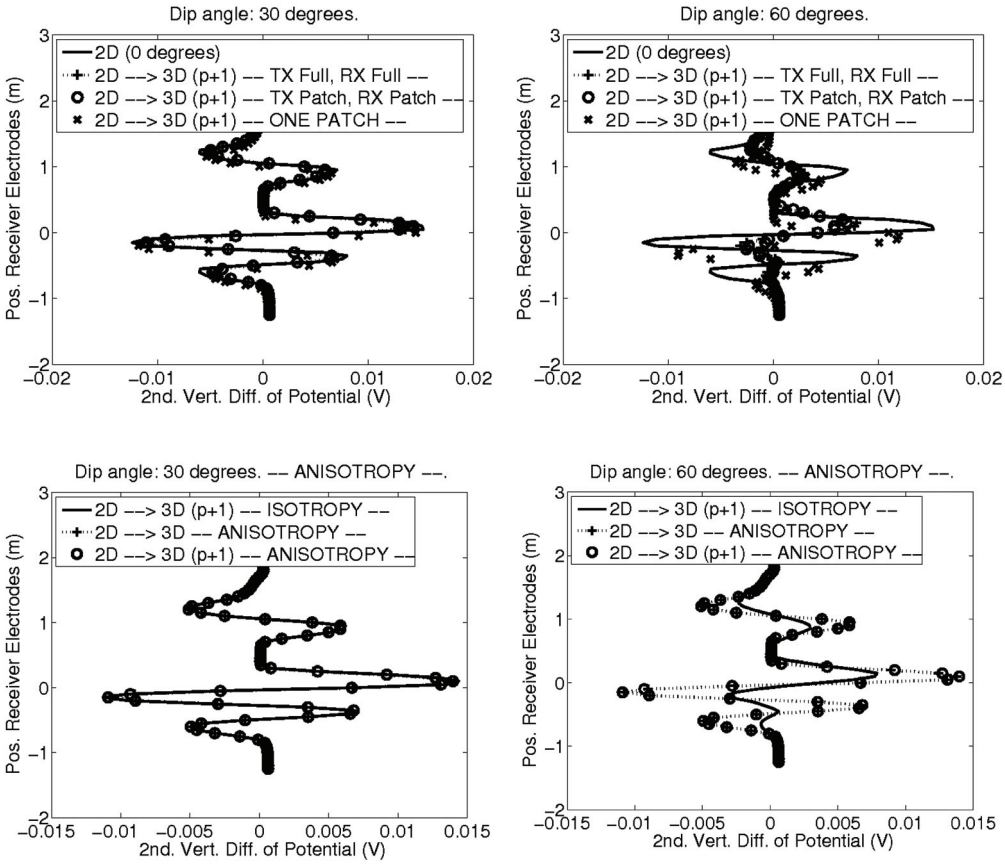

Fig. 6. LWD problem. Results obtained using an optimal 2D *hp*-FE grid transferred to the 3D software, and possibly increase globally the polynomial order of approximation *p* by one. Left panel: 30-degree deviated well; Right panel: 60-degree deviated well. Top panel: Different curves identify the following electrode configurations: A) Continuous line: 2D results for a vertical well. B) Discontinuous line with '+': full-ring electrodes. C) Circles 'o': Electrodes composed of four patches. D) Stars 'x': Electrodes composed of one-patch. Bottom panel: Different curves identify the following results: A) Continuous line: Isotropic problem. B) Discontinuous line with '+': Anisotropic problem. C) Circles 'o': Anisotropic problem, and global increase globally of the polynomial order of approximation *p* by one.

The methodology used in our simulations is based on a new 3D *hp*-FEM with exact geometry elements combined with a 2D self-adaptive goal-oriented *hp* strategy that enables simultaneous simulation of different 3D effects.

Acknowledgments

The work presented in this paper was supported by The University of Texas at Austin's *Joint Industry Research Consortium on Formation Evaluation* sponsored by Anadarko, Aramco, Baker Atlas, British Gas, BHP-Billiton, BP, Chevron, Conoco-Phillips, ENI E&P,

ExxonMobil, Halliburton, Marathon, Mexican Institute for Petroleum, Hydro, Occidental Petroleum, Petrobras, Schlumberger, Shell E&P, Statoil, TOTAL, and Weatherford International, Ltd. The second author was financially supported by the Foundation for Polish Science under program Homing.

References

[1] Zhang, R. L. Mackie, and T. R. Madden, "3-D resistivity forward modeling and inversion using conjugate gradients," *Geophysics*, vol. 60, pp. 1312–1325, 1995.

[2] V. L. Druskin, L. A. Knizhnerman, and P. Lee, "New spectral Lanczos decomposition method for induction modeling in arbitrary 3-D geometry," *Geophysics*, vol. 64, no. 3, pp. 701–706, 1999.

[3] G. A. Newman and D. L. Alumbaugh, "Three-dimensional induction logging problems, part 2: A finite-difference solution," *Geophysics*, vol. 67, no. 2, pp. 484–491, 2002.

[4] S. Davydycheva, V. Druskin, and T. Habashy, "An efficient finite-difference scheme for electromagnetic logging in 3D anisotropic inhomogeneous media," *Geophysics*, vol. 68, no. 5, pp. 1525–1536, 2003.

[5] T. Wang and S. Fang, "3-D electromagnetic anisotropy modeling using finite differences," *Geophysics*, vol. 66, no. 5, pp. 1386–1398, 2001.

[6] T. Wang and J. Signorelli, "Finite-difference modeling of electromagnetic tool response for logging while drilling," *Geophysics*, vol. 69, no. 1, pp. 152–160, 2004.

[7] D. B. Avdeev, A. V. Kuvshinov, O. V. Pankratov, and G. A. Newman, "Three-dimensional induction logging problems, part 1: An integral equation solution and model comparisons," *Geophysics*, vol. 67, pp. 413–426, 2002.

[8] A. Abubakar and P. M. van den Berg, "Nonlinear inversion in electrode logging in a highly deviated formation with invasion ising an oblique coordinate system," *IEEE Transactions on Geoscience and Remote Sensing*, vol. 38, pp. 25–38, 2000.

[9] D. Pardo, L. Demkowicz, C. Torres-Verdin, and L. Tabarovsky, "A goal-oriented - adaptive finite element method with electromagnetic applications. Part I: electrostatics," *International Journal for Numerical Methods in Engineering*, vol. 65, pp. 1269–1309, 2006.

[10] M. Paszynski, L. Demkowicz, and D. Pardo, "Verification of goal-oriented - adaptivity," *Computers and Mathematics with Applications*, vol. 50, pp. 1395–1404, 2005.

[11] Pardo, C. Torres-Verdin, and L. Demkowicz, Simulation of multi-frequency borehole resistivity measurements through metal casing using a goal-oriented hp-finite element method, IEEE Transactions on Geosciences and Remote Sensing, vol. 44, Issue 8, pp. 2125–2135, 2006.